THE JOURNAL OF PHYSICAL CHEMISTRY C
A JOURNAL OF THE AMERICAN CHEMICAL SOCIETY

pubs.acs.org/JPCC

Article

# Linker-Templated Structure Tuning of Optical Response in Plasmonic Nanoparticle Gels

*Published as part of The Journal of Physical Chemistry virtual special issue "Pablo G. Debenedetti Festschrift".*

Murari Singh,[†] Zachary M. Sherman,[†] Delia J. Milliron, and Thomas M. Truskett*

**Cite This:** *J. Phys. Chem. C* 2022, 126, 16885−16893

Read Online

ACCESS | Metrics & More | Article Recommendations

Downloaded via UNIV OF TEXAS AT AUSTIN on May 9, 2023 at 20:16:08 (UTC).
See https://pubs.acs.org/sharingguidelines for options on how to legitimately share published articles.

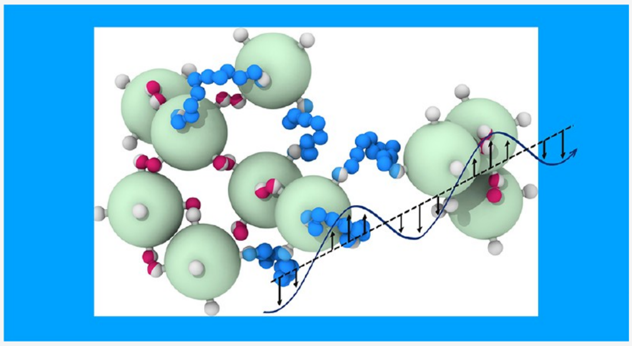

**ABSTRACT:** Gel assemblies of functional nanoparticles, reversibly associated into percolating networks using bifunctional linking molecules, offer promise as versatile materials platforms. Molecular linkers can be customized to template interparticle spacing and modify colloidal network attributes, enabling design for structure-dependent properties. Mechanical properties of gels are commonly studied by molecular simulation, but simulating the optical response of large-scale, disordered assemblies has been computationally intractable, limiting our understanding of light−matter interactions in structurally complex plasmonic networks. Here, we use a recently developed mutual polarization method, capable of predicting optical properties for large disordered configurations of spherical particles, together with an experimentally informed coarse-grained model to study the behavior of plasmonic linker gels. The simulation results demonstrate how blends of short and long linkers with the same average molecular weight can be chosen to deliberately modulate structure-dependent near- and far-field spectral features of the colloidal gel while preserving gel mechanical properties. Linker selection can also be used to prepare gel networks with qualitatively different mechano-optical responses. The structural changes occurring under strain shed light on possible origins of experimentally observed red- and blue-shifting of the optical extinction of plasmonic nanocomposites under a uniaxial extension.

## ■ INTRODUCTION

Assemblies of metal nanoparticles, whose conduction electrons interact collectively with light by localized surface plasmon resonance (LSPR), display rich optical properties.[1−4] Structure-dependent LSPR coupling in these materials produces frequency-tunable absorption and strong electromagnetic fields in gaps between closely spaced nanoparticles ("hot spots"), enabling applications from molecular detection and characterization to energy harvesting and data storage.[3,5−14] This sensitivity to nanoparticle spatial organization can render plasmonic assemblies responsive, capable of dynamically reconfiguring due to physicochemical,[15−24] electromagnetic,[21,24−29] or mechanical[30−42] stimuli to form structures with distinct optical near- and far-field spectral features.

Bifunctional molecules that link sites (e.g., ligands) on neighboring nanoparticles offer a powerful handle for design of functional colloidal assemblies. Linkers can be selected to deliberately template colloid spacing and valence in three-dimensional networks, as demonstrated for plasmonic clusters,[27,43−49] superlattices,[50−55] and gels.[22,23,56−58] In recent studies, doped metal oxide nanocrystal dispersions underwent pronounced structural changes upon linker-mediated gelation by dynamic covalent bonding,[22,23,59] and the resulting LSPR coupling led to substantial modulation of their infrared extinction spectra. Since mechanical properties of colloidal gels are also sensitive to network architecture,[60−63] linked colloidal gel assembly presents an attractive platform for preparing hybrid materials with targeted optical and mechanical properties and distinctive mechano-optical response.

Though mechanical properties of amorphous materials are commonly studied by molecular simulation, modeling the optical response of nanoparticle assemblies with complex structural features involving large numbers of particles has been computationally intractable.[59] Accordingly, how local structuring affects resonant light−matter interactions in disordered plasmonic materials such as colloidal gels with strong LSPR coupling remains poorly understood.[22,23,59] We recently introduced a highly efficient mutual polarization

**Received:** July 28, 2022
**Revised:** September 15, 2022
**Published:** September 27, 2022

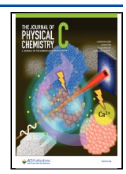


© 2022 American Chemical Society

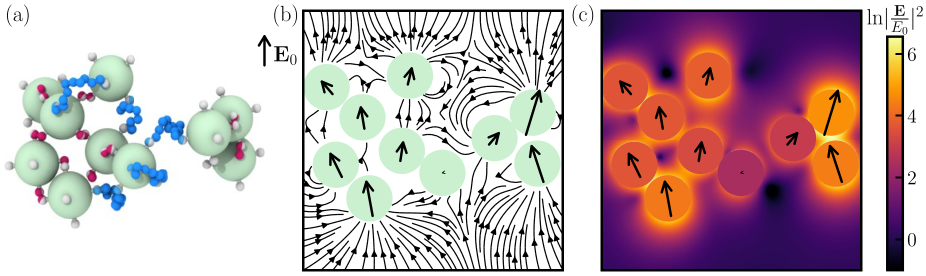


**Figure 1.** Computing the optical response of a linked nanoparticle network. (a) Assemblies are simulated using the PolyPatch model,[64,65] where nanoparticles (green) functionalized with patches (gray) are bonded to form an extended network by a blend of long (blue) and short (red) linking chains. The mutual polarization method (MPM)[59] is then used to determine the induced dipoles and the spatial distribution of the electric field in response to incident light with polarization $\mathbf{E}_0$. Particle arrows indicate the imaginary component of dipoles in (b) and (c), field lines in (b) indicate the imaginary component of the electric field, and field intensity is shown in (c).

method (MPM)[59] capable of rapidly computing optical properties for arbitrary configurations of thousands of spherical nanoparticles with periodic boundary conditions, including mixtures of colloids with different dielectric functions. Here, we use this method together with configurations generated from an experimentally informed coarse-grained model[64,65] to explore via simulation how linking molecules can be selected to deliberately modify the structure in colloidal gels for the desired optical and mechanical properties (Figure 1).

Our simulation results establish linker molecular weight distribution as a powerful tool for designing plasmonic linker gels. As previously hypothesized,[64] we found that optical extinction spectra can be tuned largely independent of gel elastic properties by employing different blends of short and long linkers with fixed average molecular weight. Short linkers strongly constrain the distance between nanoparticle surfaces they connect, creating small interparticle gaps. Increasing the proportion of these gaps strengthens LSPR coupling in the network, leading to high near-field enhancement and broadening the optical extinction spectra.[22,23,59] On the other hand, as in polymer networks,[66−69] the elastic moduli and elongation behavior of the resulting nanoparticle networks depend on average linker length, but are otherwise insensitive to the details of the linker-size distribution. Together, this modeling predicts that linker composition provides a convenient experimental handle for modulating the optical response of gels without sacrificing key aspects of their mechanical properties.

The simulations also allowed us to test how linker mixtures can be chosen to program the optical response of plasmonic gels to changes in their macroscopic strain state. Experiments on polymer−metal nanocomposites have produced qualitatively distinct polarization-dependent spectral changes due to stretching,[31,33−35,38] but detailed information about how the mechano-optical properties reflect modifications to local arrangement of nanoparticles in real-space is lacking. Unlike for nanocomposites, the plasmonic nanoparticles of linked colloidal gels are themselves elements of the percolating network, which tightly couples their spatial organization to the macroscopic strain state of the material. Using our model linker gel, we study how this coupling leads to optical responses that reproduce the diverse trends observed in experiments and relate them to linker-templated structural modifications of the networks under uniaxial strain.

## ■ METHODS

**Coarse-Grained Model.** Plasmonic nanoparticle−linker networks were studied via molecular dynamics simulations in the canonical ensemble using LAMMPS (Large-scale Atomic/Molecular Massively Parallel Simulator),[70] fixing temperature and volume $V$ of a triply periodic, square cuboid-shaped cell. Interactions were described by the coarse-grained PolyPatch (Polymer linked, Patchy colloid) model,[64,65] which treats bifunctional linking molecules as linear bead−spring chains and nanoparticles as spherical colloids with patches that can each form at most one attractive bond of strength $\varepsilon$ with a chain end (Figure 1b). Gelation occurs by slowly "cooling" a single-phase fluid to conditions of high $\beta\varepsilon$, where $\beta = 1/k_BT$ and $k_B$ is the Boltzmann constant. The mechanical response of the networks to uniaxial deformation can then be readily probed via molecular dynamics simulations.

Linkers were modeled as fully flexible chains with repulsive chain-segment interactions, mimicking good-solvent conditions,[71] and segments were treated as spherical beads of diameter $d$ and mass $m$, joined to their neighbors by finitely extensible nonlinear elastic bonds. Linker stiffness is also a tunable parameter of the PolyPatch model; a discussion about its effects on colloidal network structure and properties, as well as synthetic strategies for its systematic variation in experiments, is presented elsewhere.[65] Simulated trajectories included $N_c = 1000$ colloids with diameter $d_c = 5d$ and mass $m_c = 125m$ decorated with six linking sites (patches of diameter $d$) in an octahedral arrangement on their surfaces. We chose a stoichiometric linker-to-colloid ratio of $\Gamma \equiv N_l/N_c = 3$ (i.e., $N_l = 3000$ linkers) and a colloid volume fraction of $\eta_c = N_c\pi d_c^3/(6V) = 0.15$. We studied three systems with single-component linkers, small chains with $M = 2$, 5, and 8 segments, respectively, as well as binary linker mixtures with $\langle M\rangle \equiv (N_1M_1 + N_2M_2)/N_l = 5$, where $N_i$ represents the number of linkers (i.e., $M_i$, segment chains) of component $i$ (Table 1). Configurations were rendered using OVITO 2.9.0.[72]

**Mechanical Properties.** As described elsewhere,[64] slow annealing was used to prepare gels. Molecular dynamics simulations were initially equilibrated for $0.5 \times 10^4\ \tau$ without any linker-patch bonding ($\beta\varepsilon = 0$), where $\tau = \sqrt{\beta m d^2}$. The integration time step was 0.001 $\tau$, and $T$ was controlled by a Langevin thermostat with friction coefficient 0.1 $m/\tau$ applied to each particle. Linker-patch bonding energy was increased to $\beta\varepsilon = 10$ over $10^4\ \tau$, followed by a $10^4\ \tau$ equilibration period. Linker-patch energy was then further ramped by $k_BT$ over a 0.5


https://doi.org/10.1021/acs.jpcc.2c05353
J. Phys. Chem. C 2022, 126, 16885−16893

**Table 1. Number of Chain Segments for Short and Long Linkers, $M_1$ and $M_2$, Respectively, Linker Number Ratio $N_1/N_2$, and Average Chain Length $\langle M \rangle$ for Binary Linker Mixtures**

| $M_1$ | $M_2$ | $N_1/N_2$ | $\langle M \rangle$ |
|---|---|---|---|
| 2 | | 100:0 | 2 |
| 8 | | 100:0 | 8 |
| 5 | | 100:0 | 5 |
| 2 | 8 | 50:50 | 5 |
| 2 | 10 | 62.5:37.5 | 5 |
| 2 | 12 | 70:30 | 5 |

$\times$ $10^4$ $\tau$ period, followed by reequilibration for $1.5 \times 10^4$ $\tau$. This process was repeated nine times to reach $\beta\varepsilon = 20$. Final configurations saved from this annealing protocol were thermalized for $2 \times 10^3\tau$ at $\beta\varepsilon = 100$ and subsequently used as the initial states for the uniaxial elongation simulations described below. In the gel states, over 85% of linkers formed bridges between patches on neighboring nanoparticles, while the rest either bonded to a single patch (with a dangling end) or bonded to two patches on the same colloid, forming a self-loop. No self-loops form for $M$ = 2 and 5 linkers because their end-to-end distance is shorter than the patch−patch separation on a colloid.

To quantify the mechanical response of gels to uniaxial extension, we performed a series of deformation simulations in which one dimension of the simulation cell $L_z$ was elongated at a steady rate of $10^{-4}$ $\tau^{-1}$. The other two dimensions, $L_x$ and $L_y$, were simultaneously and isotropically contracted at a rate to conserve volume, consistent with a Poisson's ratio of 1/2 (commonly observed for soft materials like polymer melts and solutions, where the bulk modulus is higher than the shear modulus).[71] Strains in the range $\lambda = L_z/L_{z,0} \in [1, 4]$ were simulated, where $L_{z,0}$ was the initial box dimension in the $z$ direction. Bonds between linkers and patches break and reform during deformation. The engineering (or nominal) stress was computed from the diagonal components of stress tensor, $\sigma_n \equiv \sigma_{\text{true}}/\lambda = [\sigma_{zz} - 0.5(\sigma_{xx} + \sigma_{yy})]/\lambda$, where $\sigma_{\text{true}}$ is the true stress. For small uniaxial deformations, the simulation data obeys the classical form of the stress−elongation relationship, $\sigma_{\text{eng}} = G(\lambda - 1/\lambda^2)$, observed experimentally for polymer networks and predicted by network elasticity theory.[71] Using this form, we extracted $G$ from simulated uniaxial elongation data, averaging over 10 independent initial configurations and deformations in three independent deformation directions ($x$, $y$, and $z$). From the averaged $\sigma_n$ across samples, we extract the maximum stress $\sigma_n^{\text{UTS}}$ and corresponding strain $\lambda^{\text{UTE}}$.

**Optical Properties.** We calculated the extinction spectra and distributions of near-field intensity for our simulated nanoparticle networks using a recently developed many-bodied, mutual polarization method (MPM) .[59] The dielectric function of the plasmonic colloids are modeled with a Drude dielectric function, $\varepsilon_p(\omega) = \varepsilon_\infty - \varepsilon_0\omega_p^2/(\omega^2 + i\gamma\omega)$, where $\omega_p$ is the plasma frequency, $\gamma$ is the damping coefficient, $\varepsilon_\infty$ is the high-frequency permittivity, and $\varepsilon_0$ is the vacuum permittivity. The permittivity of the background medium $\varepsilon_m$ is assumed real and frequency-independent over the range of interest. The patches and linkers are ignored in the optical calculations. We set $\gamma = 0.05\omega_p^*$ and $\varepsilon_\infty = 2\varepsilon_m$, where $\omega_p^* = \omega_p\sqrt{\varepsilon_0/\varepsilon_m}$ is an effective plasma frequency. For generality, extinction spectra are shown in terms of a dimensionless extinction cross-section per nanoparticle volume $C/(\sqrt{\varepsilon_m\mu_m}\,\omega_p^*)$ as a function of dimensionless frequency $\omega/\omega_p^*$, where $\mu_m$ is permeability of the background medium. In terms of these units, the optical calculations apply to a range of materials, with different colloid compositions and background media encoded through specific choices of $\omega_p^*$ and $\varepsilon_m$. For example, typical values for colloidal tin-doped indium oxide (ITO) nanoparticles are $\varepsilon_m = 2\varepsilon_0$, $\omega_p^* = 10000$ cm$^{-1}$, $\gamma = 500$ cm$^{-1}$, and $\varepsilon_\infty = 4\varepsilon_0$.

The $N$ induced particle dipoles $\mathbf{p}_i$ in an electric field $\mathbf{E}_0$ of magnitude $E_0 = |\mathbf{E}_0|$ are computed by solving the linear system of equations for each frequency $\omega$

$$\mathbf{E}_0 = \sum_j \mathbf{M}_{ij}\cdot\mathbf{p}_j \tag{1}$$

where

$$\mathbf{M}_{ij} = \begin{cases} \dfrac{1}{\varepsilon_m\alpha}\mathbf{I} & i = j \\ \dfrac{1}{4\pi\varepsilon_m r^3}(\mathbf{I} - 3\hat{\mathbf{r}}\hat{\mathbf{r}}) & i \neq j,\ r \geq d_c \\ \dfrac{2}{\pi d_c^3\varepsilon_m}\left[\left(1 - \dfrac{9r}{8d_c} + \dfrac{r^3}{4d_c^3}\right)\mathbf{I} + \left(\dfrac{3r^3}{4d_c^3} - \dfrac{9r}{8d_c}\right)\hat{\mathbf{r}}\hat{\mathbf{r}}\right] & i \neq j,\ r < d_c \end{cases} \tag{2}$$

$\alpha(\omega) = \frac{1}{2}\pi d_c^3(\varepsilon_p(\omega) - \varepsilon_m)/(\varepsilon_p(\omega) + 2\varepsilon_m)$ is the dipole polarizability, $d_c$ is the particle diameter, $\varepsilon_p(\omega)$ is the particle permittivity at $\omega$, $\varepsilon_m$ is the permittivity of the background medium (assumed pure real), $\mathbf{r} = \mathbf{x}_i - \mathbf{x}_j$, $\mathbf{x}_i$ is particle $i$'s position, $r = |\mathbf{r}|$, $\hat{\mathbf{r}} = \mathbf{r}/r$, and $\mathbf{I}$ is the identity tensor. The sum in eq 1 runs over all particles and their periodic images and is evaluated using an efficient Ewald summation method.[73] This linear system is solved iteratively using the generalized minimal residual method (GMRES) to a relative error tolerance of $10^{-3}$. The ensemble-averaged extinction cross-section per nanoparticle volume is

$$C = \frac{6\sqrt{\mu_m}\,\omega}{\pi d_c^3\sqrt{\varepsilon_m}\,E_0^2}\mathrm{Im}[\langle\mathbf{p}\rangle\cdot\mathbf{E}_0] \tag{3}$$

where $\langle\mathbf{p}\rangle = \sum_i \mathbf{p}_i/N$ is the ensemble-averaged dipole. If $C^{(i)}$ is the ensemble-averaged extinction cross-section for a particular field polarization $\mathbf{E}_0 = E_0\hat{\mathbf{e}}_i$, the polarization-averaged extinction cross-section is $C = \sum_i C^{(i)}/N_E$, where $N_E$ is the number of polarizations. The local field at any point $\mathbf{x}$ is

$$\mathbf{E}(\mathbf{x}) = \begin{cases} \mathbf{E}_0 + \displaystyle\sum_j \frac{1}{4\pi\varepsilon_m r^3}(3\hat{\mathbf{r}}\hat{\mathbf{r}} - \mathbf{I})\cdot\mathbf{p}_j, & \mathbf{x} \text{ in medium} \\ \dfrac{6\mathbf{p}_i}{\pi d_c^3(\varepsilon_p - \varepsilon_f)}, & \mathbf{x} \text{ in particle } i \end{cases} \tag{4}$$

where the sum runs over all particles and periodic images and is evaluated using the same Ewald method as eq 1. The locations of local maxima in the field intensity, that is, "hot-spots", are approximated as $\mathbf{x}_{i,\text{hot}} = \mathbf{x}_i \pm \frac{d_c}{2}\mathrm{Im}\hat{\mathbf{p}}_i$, and the collection of $2N$ values for $|\mathbf{E}(\mathbf{x}_{i,\text{hot}})|$ make up the field distribution for a single polarization and configuration.


https://doi.org/10.1021/acs.jpcc.2c05353
J. Phys. Chem. C 2022, 126, 16885−16893

For quiescent gels, extinction spectra and the near-field distributions are averaged over $x$, $y$, and $z$ polarizations and 10 gel configurations from independent molecular dynamics simulations. The near-field distributions are sampled at the frequency corresponding to maximum $|\langle \mathbf{p} \rangle|$ for each gel. For strained gels, perpendicular-polarization extinction spectra are averaged over two polarizations ($E_0\hat{\mathbf{e}}_x$ and $E_0\hat{\mathbf{e}}_y$) perpendicular to the elongation axis ($\hat{\mathbf{e}}_z$). Both the parallel- and perpendicular-polarization extinction spectra are averaged over 10 independent trajectories at each strain value, and $\omega_{\mathrm{LSPR}}$ is the frequency corresponding to the maximum value of the extinction spectra.

**Structural Properties.** The directional radial distribution functions $g_{\parallel}$ and $g_{\perp}$ were computed with the help of projected distances

$$r_{ij} = |\mathbf{x}_i - \mathbf{x}_j|, \quad r_{\parallel,ij} = |(\mathbf{x}_i - \mathbf{x}_j)\cdot\hat{\mathbf{e}}_z|, \quad r_{\perp,ij} = |(\mathbf{x}_i - \mathbf{x}_j)\cdot(\mathbf{I} - \hat{\mathbf{e}}_z\hat{\mathbf{e}}_z)| \tag{5}$$

The quantity $g_{\parallel}(r)$ is the radial distribution function computed only between pairs of particles with $r_{\perp} \leq d_c/2$, and $g_{\perp}(r)$ is computed only between pairs of particles with $r_{\parallel} \leq d_c/2$. We calculate these radial distribution functions through conditional binning

$$g_{\perp}(r) = \frac{1}{\rho N 4\pi r d_c h}\sum_{ij}^{N}\begin{cases}1, & r - \frac{h}{2} \leq r_{ij} < r + \frac{h}{2} \quad \text{and} \quad r_{\parallel,ij} \leq \frac{d_c}{2}\\ 0, & \text{otherwise}\end{cases} \tag{6}$$

$$g_{\parallel}(r) = \frac{2}{\rho N \pi d_c^2 h}\sum_{ij}^{N}\begin{cases}1, & \text{if} \quad r - \frac{h}{2} \leq r_{ij} < r + \frac{h}{2} \quad \text{and} \quad r_{\perp,ij} \leq \frac{d_c}{2}\\ 0, & \text{otherwise}\end{cases} \tag{7}$$

where $h = 0.004d_c$ is the bin spacing and $\rho$ is the number density.

The three-dimensional structure factor $S(\mathbf{q})$ was computed on a grid of wavevectors $\mathbf{q} = [2\pi\kappa_x/L_x, 2\pi\kappa_y/L_y, 2\pi\kappa_z/L_z]$, where $\kappa_i = -N_i/2, ..., (N_i - 1)/2$ and $L_i$ are the box dimensions, by dividing the simulation box into $N_xN_yN_z$ approximately cubic cells with centers $\mathbf{r} = [n_xL_x, n_yL_y, n_zL_z]$, where $n_i = -N_i/2, ..., (N_i - 1)/2$. Selecting $N_x = N_y = 256$ in the smallest box dimension and $N_z = N_xL_z/L_x$ (rounded to nearest integer) to maintain uniform grid density, we counted the number of particles in each cell $\rho(\mathbf{r})$, used a fast Fourier transform to get $\hat{\rho}(\mathbf{q})$, then computed $S(\mathbf{q}) = |\hat{\rho}|^2/N$. Using projected wavenumbers

$$q_{\parallel} = |\mathbf{q}\cdot\hat{\mathbf{e}}_z|, \quad q_{\perp} = |\mathbf{q}\cdot(\mathbf{I} - \hat{\mathbf{e}}_z\hat{\mathbf{e}}_z)| \tag{8}$$

we computed the 2D $S(q_{\parallel}, q_{\perp})$ by constructing a grid $[2\pi\kappa_{\parallel}/L_{\parallel}, 2\pi\kappa_{\perp}/L_{\perp}]$, where $\kappa_i = 0, 1, 2, ...,$ and averaging all $S(\mathbf{q})$ values in the same bin.

We averaged $g(r)$ over 10 independent gel trajectories and 1000 configurations per gel. $S$, $g_{\parallel}$, and $g_{\perp}$ are computed over a single gel trajectory at each strain.

## RESULTS AND DISCUSSION

Simulated uniaxial deformation of the model nanoparticle networks highlights how linker molecular weight influences mechanical properties (Figure 2). Adopting short ($M = 2$) linking molecules produced rigid assemblies with higher shear modulus $G$, but lower ultimate tensile strength $\sigma_n^{\mathrm{UTS}}$ and elongation $\lambda^{\mathrm{UTE}}$, owing to the limited extensibility of the short linkers. In contrast, employing longer, flexible linking chains ($M = 8$) resulted in a softer (lower $G$) but stronger (higher $\sigma_n^{\mathrm{UTS}}$) and more stretchable (higher $\lambda^{\mathrm{UTE}}$) network. The intermediate, 5-mer colloidal gel also exhibited considerable strength and stretchability, with a modest enhancement of rigidity compared to the 8-mer gel.

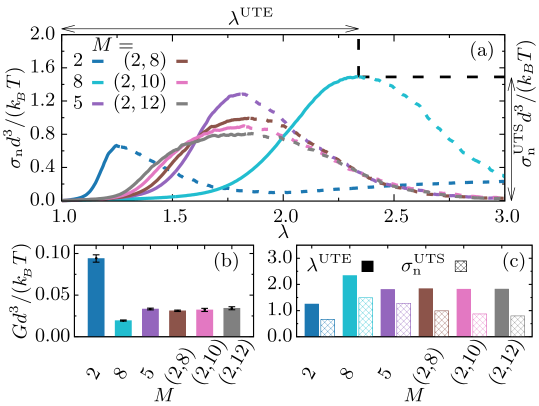


**Figure 2.** Mechanical properties of linked colloidal gels. (a) Engineering stress $\sigma_n$ in uniaxial tension version deformation $\lambda$, where $\lambda = 1$ is the unstrained state. Solid (dashed) curves show data before (after) the elongation $\lambda^{\mathrm{UTE}}$ corresponding to the ultimate tensile strength $\sigma_n^{\mathrm{UTS}}$. (b) Shear modulus $G$. Error bars indicate one standard deviation across independent samples. (c) $\sigma_n^{\mathrm{UTS}}$ and $\lambda^{\mathrm{UTE}}$. Gels with a single type of linker ($M = 2$, 5, or 8 chain segments) and binary blends with short ($M_1 = 2$) and long ($M_2 = 8$, 10, or 12) linkers, denoted ($M_1$, $M_2$) are shown.

Deformation simulations of three different colloidal networks with a fixed average linker length ($\langle M \rangle = 5$), including blends of short ($M_1 = 2$) and long ($M_2 = 8$, 10, or 12) linkers address the sensitivity of the mechanical properties to the linker size distribution. Strikingly, the computed shear modulus and ultimate elongation of these networks were equivalent to those of the 5-mer gel. The ultimate tensile strengths of the blended-linker gels were 20−35% lower than that of the 5-mer assembly and in between those of the dimer and 8-mer gels, as expected. The slightly reduced tensile strengths of blended-linker gels follows from the ability of linkers longer than $M = 5$ to form self-loops instead of bridges. These results indicate that the colloidal gels with binary linker blends show behavior consistent with experiments on polymer networks and predictions of network elasticity theory.[66−69] If the average chain length is fixed, other details of the length distribution—whether it be for polymers in a network or linkers in a colloidal gel—do not significantly impact shear elasticity or elongation behavior.

The model further suggests a design opportunity for plasmonic linker gels, where optical response is known to be sensitive to the presence of close nanoparticle separations, which give rise to pronounced LSPR coupling.[22,23] By choosing blends with different proportions of small linkers (but the same molar average linker length), it should be possible to deliberately modulate the number of close nanoparticle contacts and, hence, the structure-dependent near- and far-field optical response of the network, while leaving gel mechanical properties largely unchanged.

To elucidate how the choice of linker affects network microstructure, we computed the colloid−colloid radial distribution function $g_{cc}(r)$ (Figure 3a). The quantity

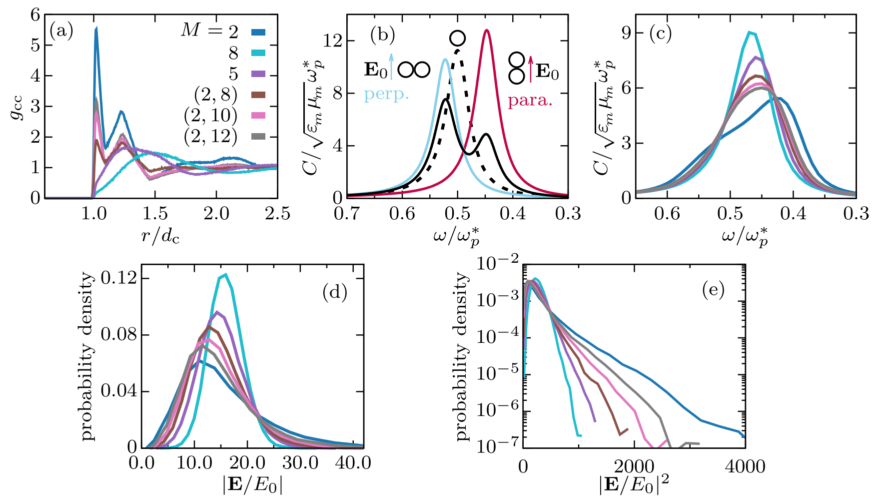


**Figure 3.** Structure and optical properties of quiescent linked colloidal gels. (a) Colloid-colloid radial distribution function, $g_{cc}$, as a function of interparticle separation $r/d_c$. (b) Extinction cross section per nanoparticle volume $C$ scaled by $\sqrt{\varepsilon_m \mu_m}\,\omega_p^*$ as a function of scaled frequency $\omega/\omega_p^*$ for a single isolated nanoparticle (dashed black), isolated contact pairs (i.e., $r = d_c$) aligned parallel and perpendicular to the incident electric field polarization, and an isolated contact pair with an isotropic distribution of orientations (solid black). (c) Gel extinction spectra. (d, e) Probability distribution of near-field $|\mathbf{E}|$ and $|\mathbf{E}|^2$ hot-spots on nanoparticle surfaces, sampled at the frequency of maximum $|\langle \mathbf{p} \rangle|$ for each gel. Data for gels with a single type of linker ($M$ = 2, 5, or 8 chain segments) and binary blends with short ($M_1$ = 2) and long ($M_2$ = 8, 10, or 12) linkers, denoted ($M_1$, $M_2$), are shown.

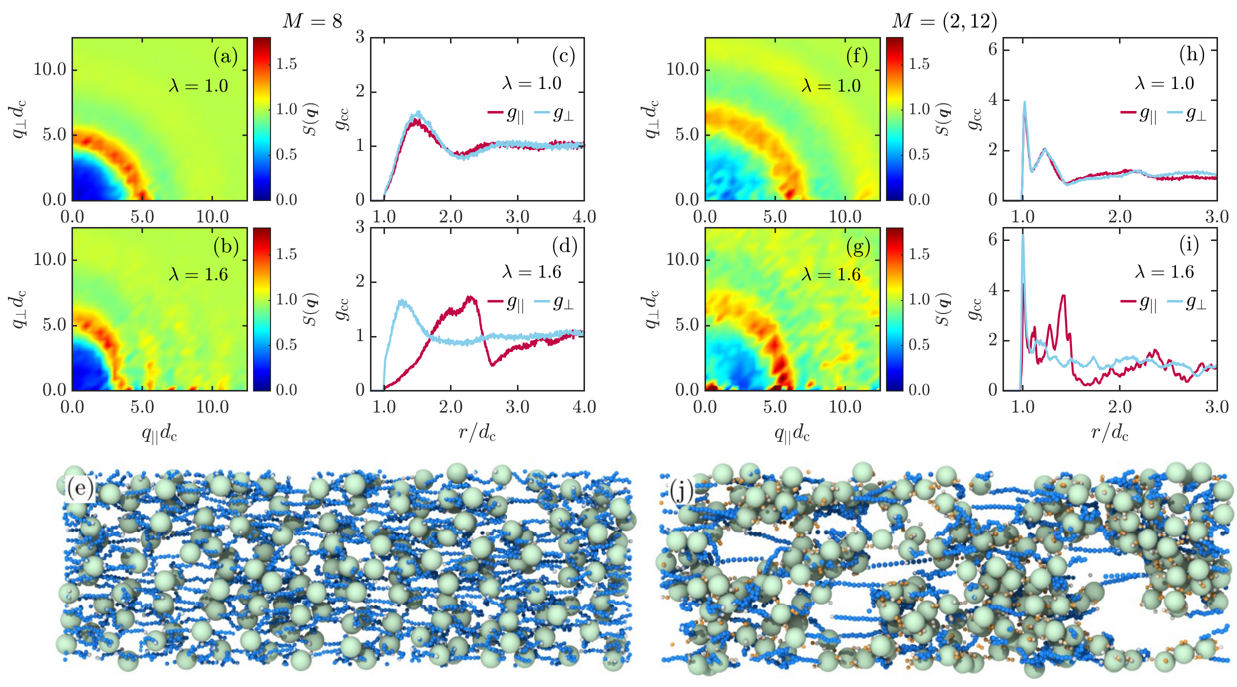


**Figure 4.** Microstructural response to uniaxial deformation for the $M$ = 8 gel (left) and the $M$ = (2, 12) mixed linker gel (right). Colloid−colloid static structure factors $S(\boldsymbol{q})$ for wavevectors parallel $q_{||}$ and perpendicular $q_{\perp}$ to strain direction: (a, f) prior to strain and (b, g) in strain. Colloid−colloid one-dimensional radial distribution function parallel $g_{||}(r)$ and perpendicular $g_{\perp}(r)$ to strain direction: (c, h) prior to strain and (d, i) in strain. Configuration snapshots in strain (e, j).

$N_c g_{cc}(r)/V$ characterizes the average colloid number density a distance $r$ away from a colloid center. Focusing on assemblies with a single linker type, there is stark, qualitative difference between the spacing of colloids when short ($M$ = 2) or longer ($M$ = 5 and 8) linkers are employed. The short-linker network's radial distribution function features a sharp colloid−colloid "contact" peak and a nearby second peak corresponding to colloid surfaces separated by the dimer bond.[64] Gels with only longer linkers lacked the contact peak altogether and instead displayed a broader first peak at larger separations, allowing the $M$ = 5 and $M$ = 8 chains to access more configurational degrees of freedom in extended states.[71] Significantly, networks with binary linker mixtures all exhibited the contact peak, the magnitude of which was correlated to the proportion of short linkers present.

The linker-templated structural differences produced a diverse range of far-field optical responses as reflected by the computed extinction cross section $C(\omega)$ (Figure 3b,c). The 8-



https://doi.org/10.1021/acs.jpcc.2c05353
J. Phys. Chem. C 2022, 126, 16885−16893

mer gel exhibited a symmetric extinction spectrum resembling the isolated particle spectrum in Figure 3b, consistent with weak LSPR coupling and expected based on the lack of a contact peak in $g_{cc}(r)$. By comparison, the extinction cross section for the dimer gel was significantly broadened, reflecting strong LSPR coupling. This broadening embodies far-field signatures of both red-shifting and blue-shifting, consistent with a structure that contains contact pairs with an isotropic distribution of orientations relative to the incident field (Figure 3b). As expected, the 5-mer and binary linker gels displayed cross sections consistent with LSPR coupling-induced broadening intermediate to that of the 8-mer and dimer networks.

Despite similarities in the far-field optical properties of the 5-mer and the binary linker networks, differences become apparent upon examination of their near-field responses (Figure 3d,e). Assemblies with linker mixtures have an increased probability of finding nanoparticles with strong local electric fields near their surfaces. Near-field enhancements were systematically more pronounced for networks with greater proportions of short linkers and hence a higher prevalence of nanoparticles in contact, that is, higher values of $g_{cc}(r = d_c)$. That hot-spot enhancements can be realized without sacrificing network stiffness or stretchability (Figure 2) emphasizes an interesting advantage of adopting blends of short and long linkers for designing plasmonic nanoparticle linker gels.

Differences in the linker-templated structure for the gels also set the stage for distinct responses to mechanical deformation (Figure 4). For the 8-mer gel network, the static structure factor and the one-dimensional colloid radial distribution functions established that strain distorts the first-neighbor coordination shell, significantly increasing nearest-neighbor distances parallel to strain, while slightly decreasing separations in the perpendicular direction. Inspection of a strained configuration confirmed that these structural changes approximately correspond to affine, uniaxial deformation. For the mixed $M = (2, 12)$ linker gel, qualitatively different deformation-induced structural changes were evident. Despite little change in the perpendicular direction, deformation enhanced structural correlations in the direction parallel to stretching, as evidenced by an increase in height of the static structure factor and the development of short-range ordering reminiscent of cluster formation in the radial distribution function.[74] The configuration snapshot of the mixed linker gel visually confirms that its structural changes reflect a spatially heterogeneous nanoparticle distribution (Figure 4j). Short linkers promote clustering of plasmonic nanoparticles under uniaxial deformation, while longer linkers extend to accommodate the macroscopic strain in the network.

Accordingly, the computed optical extinction cross sections of our model gels display distinct polarization-dependent responses to uniaxial strain, evidenced by qualitatively different shifts in their LSPR peak frequencies (Figure 5). For the 8-mer gel, the extinction maximum showed blue-shifting for the polarization parallel to the extension direction, and moderate red-shifting for the perpendicular polarization. This is behavior anticipated with affine deformation[75] such as that seen in Figure 4 for the 8-mer gel, with particles moving farther apart in the direction parallel to extension (weakening LSPR coupling), but closer together in the perpendicular direction (strengthening LSPR coupling). Though experimental systems have been prepared that show this intuitive behavior,[35,38] the opposite trend, pronounced red-shifting of the LSPR peak frequency for the parallel polarization and moderate blue-shifting in the perpendicular polarization, is more commonly observed for nanocomposites,[31,40−42] where the plasmonic nanoparticles have a tendency to cluster. The simulated colloidal gel with a binary mixture of $M_1 = 2$ and $M_2 = 12$ linkers, which also formed nanoparticle clusters under uniaxial strain (Figure 4), displayed this more typical, though less intuitive, mechano-optical response (Figure 5b). Unlike in the plasmonic nanocomposites, where the degree of nanoparticle clustering and structure-dependent optical response is extremely challenging to control, the present results suggest that such changes can be deliberately engineered in linked plasmonic nanoparticle networks via a macroscopic control parameter: the proportion of short linkers (i.e., the composition of the binary linker blend).

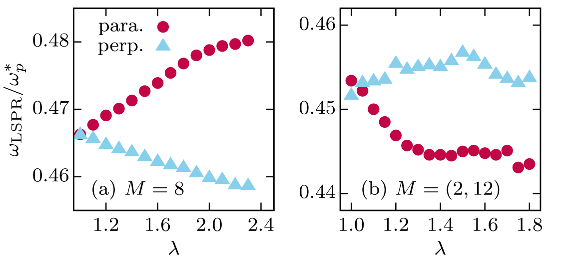


**Figure 5.** Shifts of the polarization-dependent LSPR frequency $\omega_{\mathrm{LSPR}}$ due to uniaxial strain. Parallel (circle) and perpendicular (triangle) polarizations shown for (a) the $M = 8$ and (b) the $M = (2, 12)$ mixed linker networks.

## ■ CONCLUSIONS

The simulation results reported here, leveraging the recently introduced MPM for computing optical properties of disordered assemblies[59] and the experimentally motivated coarse-grained PolyPatch model,[64,65] establish how binary mixtures of short and long linkers can be chosen to deliberately template structure and modulate near- and far-field optical and mechano-optical responses of plasmonic nanoparticle linker gels. By changing the composition in a blend of short and long linkers, one can assemble plasmonic networks with qualitatively different mechano-optical responses, capturing the diversity of behaviors observed in experiments and providing insights into their structural origins. This framework can be extended in future studies, and even coupled with inverse methods,[76] to design assembly of complex plasmonic gels with novel structure-dependent properties, including hierarchical networks with planet-satellite motifs[77] or interlaced double networks.[78] It should also prove useful for studying linker-templated compositional ordering and optical response of binary plasmonic nanoparticle gels, complementing what is known about plasmon coupling in binary nanocrystal superlattices.[59,79−82] Finally, it may be interesting to consider networks with a much wider range of linker molecular weights and linker-to-colloid ratios, for example, characterizing both Poisson's ratio and optical response in plasmonic composites mimicking the behavior of hyper-auxetic networks with ultralow cross-linking density.[83]

## ■ AUTHOR INFORMATION

### Corresponding Author

**Thomas M. Truskett** − *McKetta Department of Chemical Engineering, University of Texas at Austin, Austin, Texas 78712, United States; Department of Physics, University of*


https://doi.org/10.1021/acs.jpcc.2c05353
J. Phys. Chem. C 2022, 126, 16885−16893

Texas at Austin, Austin, Texas 78712, United States; orcid.org/0000-0002-6607-6468; Email: truskett@che.utexas.edu

### Authors

**Murari Singh** − *McKetta Department of Chemical Engineering, University of Texas at Austin, Austin, Texas 78712, United States*

**Zachary M. Sherman** − *McKetta Department of Chemical Engineering, University of Texas at Austin, Austin, Texas 78712, United States;* orcid.org/0000-0001-9798-287X

**Delia J. Milliron** − *McKetta Department of Chemical Engineering, University of Texas at Austin, Austin, Texas 78712, United States; Department of Chemistry, University of Texas at Austin, Austin, Texas 78712, United States;* orcid.org/0000-0002-8737-451X

Complete contact information is available at: https://pubs.acs.org/10.1021/acs.jpcc.2c05353

### Author Contributions

†These authors contributed equally to the work.

### Notes

The authors declare no competing financial interest.

## ■ ACKNOWLEDGMENTS

This research was primarily supported by the National Science Foundation through the Center for Dynamics and Control of Materials: an NSF Materials Research Science and Engineering Center (NSF MRSEC) under Cooperative Agreement DMR-1720595. This work was also supported by the Welch Foundation (F-1848 and F-1696), and an Arnold O. Beckman Postdoctoral Fellowship to Z.M.S. We thank the Texas Advanced Computing Center (TACC) at the University of Texas at Austin for HPC resources.

## ■ REFERENCES

(1) Halas, N. J.; Lal, S.; Chang, W.-S.; Link, S.; Nordlander, P. Plasmons in strongly coupled metallic nanostructures. *Chem. Rev.* **2011**, *111*, 3913−3961.

(2) Ross, M. B.; Mirkin, C. A.; Schatz, G. C. Optical properties of one-, two-, and three-dimensional arrays of plasmonic nanostructures. *J. Phys. Chem. C* **2016**, *120*, 816−830.

(3) Kravets, V. G.; Kabashin, A. V.; Barnes, W. L.; Grigorenko, A. N. Plasmonic surface lattice resonances: a review of properties and applications. *Chem. Rev.* **2018**, *118*, 5912−5951.

(4) Agrawal, A.; Cho, S. H.; Zandi, O.; Ghosh, S.; Johns, R. W.; Milliron, D. J. Localized surface plasmon resonance in semiconductor nanocrystals. *Chem. Rev.* **2018**, *118*, 3121−3207.

(5) Chen, H.-Y.; Lin, M.-H.; Wang, C.-Y.; Chang, Y.-M.; Gwo, S. Large-scale hot spot engineering for quantitative SERS at the single-molecule scale. *J. Am. Chem. Soc.* **2015**, *137*, 13698−13705.

(6) Matricardi, C.; Hanske, C.; Garcia-Pomar, J. L.; Langer, J.; Mihi, A.; Liz-Marzan, L. M. Gold nanoparticle plasmonic superlattices as surface-enhanced Raman spectroscopy substrates. *ACS Nano* **2018**, *12*, 8531−8539.

(7) Le, F.; Brandl, D. W.; Urzhumov, Y. A.; Wang, H.; Kundu, J.; Halas, N. J.; Aizpurua, J.; Nordlander, P. Metallic nanoparticle arrays: a common substrate for both surface-enhanced Raman scattering and surface-enhanced infrared absorption. *ACS Nano* **2008**, *2*, 707−718.

(8) Maier, S. A.; Atwater, H. A. Plasmonics: Localization and guiding of electromagnetic energy in metal/dielectric structures. *J. Appl. Phys.* **2005**, *98*, 011101.

(9) Beck, F.; Polman, A.; Catchpole, K. Tunable light trapping for solar cells using localized surface plasmons. *J. Appl. Phys.* **2009**, *105*, 114310.

(10) Linic, S.; Christopher, P.; Ingram, D. B. Plasmonic-metal nanostructures for efficient conversion of solar to chemical energy. *Nat. Mater.* **2011**, *10*, 911−921.

(11) Atwater, H. A.; Polman, A. Plasmonics for improved photovoltaic devices. *Nat. Mater.* **2010**, *9*, 205−2013.

(12) Cui, J.; Li, Y.; Liu, L.; Chen, L.; Xu, J.; Ma, J.; Fang, G.; Zhu, E.; Wu, H.; Zhao, L.; et al. Near-infrared plasmonic-enhanced solar energy harvest for highly efficient photocatalytic reactions. *Nano Lett.* **2015**, *15*, 6295−6301.

(13) Hou, W.; Cronin, S. B. A review of surface plasmon resonance-enhanced photocatalysis. *Adv. Funct. Mater.* **2013**, *23*, 1612−1619.

(14) Kristensen, A.; Yang, J. K.; Bozhevolnyi, S. I.; Link, S.; Nordlander, P.; Halas, N. J.; Mortensen, N. A. Plasmonic colour generation. *Nat. Rev. Mater.* **2016**, *2*, 1−14.

(15) Moaseri, E.; Bollinger, J. A.; Changalvaie, B.; Johnson, L.; Schroer, J.; Johnston, K. P.; Truskett, T. M. Reversible self-assembly of glutathione-coated gold nanoparticle clusters via pH-tunable interactions. *Langmuir* **2017**, *33*, 12244−12253.

(16) Lin, Q.-Y.; Mason, J. A.; Li, Z.; Zhou, W.; O'Brien, M. N.; Brown, K. A.; Jones, M. R.; Butun, S.; Lee, B.; Dravid, V. P.; et al. Building superlattices from individual nanoparticles via template-confined DNA-mediated assembly. *Science* **2018**, *359*, 669−672.

(17) Liu, D.; Fang, L.; Zhou, F.; Li, H.; Zhang, T.; Li, C.; Cai, W.; Deng, Z.; Li, L.; Li, Y. Ultrasensitive and stable Au dimer-based colorimetric sensors using the dynamically tunable gap-dependent plasmonic coupling optical properties. *Adv. Funct. Mater.* **2018**, *28*, 1707392.

(18) Liu, L.; Gao, Z.; Jiang, B.; Bai, Y.; Wang, W.; Yin, Y. Reversible assembly and dynamic plasmonic tuning of Ag nanoparticles enabled by limited ligand protection. *Nano Lett.* **2018**, *18*, 5312−5318.

(19) Sánchez-Iglesias, A.; Claes, N.; Solís, D. M.; Taboada, J. M.; Bals, S.; Liz-Marzán, L. M.; Grzelczak, M. Reversible clustering of gold nanoparticles under confinement. *Angew. Chem., Int. Ed.* **2018**, *130*, 3237−3240.

(20) Liu, L.; Aleisa, R.; Zhang, Y.; Feng, J.; Zheng, Y.; Yin, Y.; Wang, W. Dynamic color-switching of plasmonic nanoparticle films. *Angew. Chem., Int. Ed.* **2019**, *58*, 16307−16313.

(21) Homaeigohar, S.; Elbahri, M. Switchable plasmonic nano-composites. *Adv. Opt. Mater.* **2019**, *7*, 1801101.

(22) Dominguez, M. N.; Howard, M. P.; Maier, J. M.; Valenzuela, S. A.; Sherman, Z. M.; Reuther, J. F.; Reimnitz, L. C.; Kang, J.; Cho, S. H.; Gibbs, S. L.; et al. Assembly of linked nanocrystal colloids by reversible covalent bonds. *Chem. Mater.* **2020**, *32*, 10235−10245.

(23) Kang, J.; Valenzuela, S. A.; Lin, E. Y.; Dominguez, M. N.; Sherman, Z. M.; Truskett, T. M.; Anslyn, E. V.; Milliron, D. J. Colorimetric quantification of linking in thermoreversible nanocrystal gel assemblies. *Sci. Adv.* **2022**, *8*, eabm7364.

(24) Lee, S.; Sim, K.; Moon, S. Y.; Choi, J.; Jeon, Y.; Nam, J.-M.; Park, S.-J. Controlled assembly of plasmonic nanoparticles: From static to dynamic nanostructures. *Adv. Mater.* **2021**, *33*, 2007668.

(25) Pastoriza-Santos, I.; Kinnear, C.; Pérez-Juste, J.; Mulvaney, P.; Liz-Marzán, L. M. Plasmonic polymer nanocomposites. *Nat. Rev. Mater.* **2018**, *3*, 375−391.

(26) Kundu, P. K.; Samanta, D.; Leizrowice, R.; Margulis, B.; Zhao, H.; Börner, M.; Udayabhaskararao, T.; Manna, D.; Klajn, R. Light-controlled self-assembly of non-photoresponsive nanoparticles. *Nat. Chem.* **2015**, *7*, 646−652.

(27) Jung, H.; Cha, H.; Lee, D.; Yoon, S. Bridging the nanogap with light: continuous tuning of plasmon coupling between gold nanoparticles. *ACS Nano* **2015**, *9*, 12292−12300.

(28) Yan, Y.; Chen, J. I.; Ginger, D. S. Photoswitchable oligonucleotide-modified gold nanoparticles: Controlling hybridization stringency with photon dose. *Nano Lett.* **2012**, *12*, 2530−2536.

(29) Klajn, R.; Wesson, P. J.; Bishop, K. J. M.; Grzybowski, B. A. Writing self-erasing images using metastable nanoparticle "inks". *Angew. Chem., Int. Ed.* **2009**, *48*, 7035−7039.

(30) Hsu, S.-W.; Rodarte, A. L.; Som, M.; Arya, G.; Tao, A. R. Colloidal Plasmonic Nanocomposites: From Fabrication to Optical Function. *Chem. Rev.* **2018**, *118*, 3100−3120.



https://doi.org/10.1021/acs.jpcc.2c05353
J. Phys. Chem. C 2022, 126, 16885−16893

(31) Yadav, P. R.; Rizvi, M. H.; Kuttich, B.; Mishra, S. R.; Chapman, B. S.; Lynch, B. B.; Kraus, T.; Oldenburg, A. L.; Tracy, J. B. Plasmon-coupled gold nanoparticles in stretched shape-memory polymers for mechanical/thermal sensing. *ACS Appl. Nano Mater.* **2021**, *4*, 3911−3921.

(32) Kim, Y.; Yeom, B.; Arteaga, O.; Yoo, S. J.; Lee, S.-G.; Kim, J.-G.; Kotov, N. A. Reconfigurable chiroptical nanocomposites with chirality transfer from the macro-to the nanoscale. *Nat. Mater.* **2016**, *15*, 461−468.

(33) Minnai, C.; Milani, P. Metal-polymer nanocomposite with stable plasmonic tuning under cyclic strain conditions. *Appl. Phys. Lett.* **2015**, *107*, 073106.

(34) Minnai, C.; Di Vece, M.; Milani, P. Mechanical-optical-electro modulation by stretching a polymer-metal nanocomposite. *Nanotechnology* **2017**, *28*, 355702.

(35) Cataldi, U.; Caputo, R.; Kurylyak, Y.; Klein, G.; Chekini, M.; Umeton, C.; Bürgi, T. Growing gold nanoparticles on a flexible substrate to enable simple mechanical control of their plasmonic coupling. *J. Mater. Chem. C* **2014**, *2*, 7927−7933.

(36) Bian, K.; Singh, A. K.; Hennig, R. G.; Wang, Z.; Hanrath, T. The nanocrystal superlattice pressure cell: a novel approach to study molecular bundles under uniaxial compression. *Nano Lett.* **2014**, *14*, 4763−4766.

(37) Malek, S. C.; Ee, H.-S.; Agarwal, R. Strain multiplexed metasurface holograms on a stretchable substrate. *Nano Lett.* **2017**, *17*, 3641−3645.

(38) Sannomiya, T.; Hafner, C.; Vörös, J. Strain mapping with optically coupled plasmonic particles embedded in a flexible substrate. *Opt. Lett.* **2009**, *34*, 2009−2011.

(39) Aksu, S.; Huang, M.; Artar, A.; Yanik, A. A.; Selvarasah, S.; Dokmeci, M. R.; Altug, H. Flexible plasmonics: Flexible plasmonics on unconventional and nonplanar substrates. *Adv. Mater.* **2011**, *23*, 4421−4421.

(40) Pucci, A.; Bernabò, M.; Elvati, P.; Meza, L. I.; Galembeck, F.; de Paula Leite, C. A.; Tirelli, N.; Ruggeri, G. Photoinduced formation of gold nanoparticles into vinyl alcohol based polymers. *J. Mater. Chem.* **2006**, *16*, 1058−1066.

(41) Uhlenhaut, D. I.; Smith, P.; Caseri, W. Color switching in gold—polysiloxane elastomeric nanocomposites. *Adv. Mater.* **2006**, *18*, 1653−1656.

(42) Dirix, Y.; Bastiaansen, C.; Caseri, W.; Smith, P. Oriented pearl-necklace arrays of metallic nanoparticles in polymers: a new route toward polarization-dependent color filters. *Adv. Mater.* **1999**, *11*, 223−227.

(43) Mirkin, C. A.; Letsinger, R. L.; Mucic, R. C.; Storhoff, J. J. A DNA-based method for rationally assembling nanoparticles into macroscopic materials. *Nature* **1996**, *382*, 607−609.

(44) Alivisatos, A. P.; Johnsson, K. P.; Peng, X.; Wilson, T. E.; Loweth, C. J.; Bruchez, M. P.; Schultz, P. G. Organization of 'nanocrystal molecules' using DNA. *Nature* **1996**, *382*, 609−611.

(45) Xu, X.; Rosi, N. L.; Wang, Y.; Huo, F.; Mirkin, C. A. Asymmetric functionalization of gold nanoparticles with oligonucleotides. *J. Am. Chem. Soc.* **2006**, *128*, 9286−9287.

(46) Lee, J.-H.; Nam, J.-M.; Jeon, K.-S.; Lim, D.-K.; Kim, H.; Kwon, S.; Lee, H.; Suh, Y. D. Tuning and maximizing the single-molecule surface-enhanced Raman scattering from DNA-tethered nanodumbbells. *ACS Nano* **2012**, *6*, 9574−9584.

(47) Cha, H.; Yoon, J. H.; Yoon, S. Probing quantum plasmon coupling using gold nanoparticle dimers with tunable interparticle distances down to the subnanometer range. *ACS Nano* **2014**, *8*, 8554−8563.

(48) Jones, M. R.; Seeman, N. C.; Mirkin, C. A. Programmable materials and the nature of the DNA bond. *Science* **2015**, *347*, 1260901.

(49) Rogers, W. B.; Shih, W. M.; Manoharan, V. N. Using DNA to program the self-assembly of colloidal nanoparticles and microparticles. *Nat. Rev. Mater.* **2016**, *1*, 1−14.

(50) Park, S. Y.; Lytton-Jean, A. K.; Lee, B.; Weigand, S.; Schatz, G. C.; Mirkin, C. A. DNA-programmable nanoparticle crystallization. *Nature* **2008**, *451*, 553−556.

(51) Xiong, H.; van der Lelie, D.; Gang, O. DNA linker-mediated crystallization of nanocolloids. *J. Am. Chem. Soc.* **2008**, *130*, 2442−2443.

(52) Zhang, Y.; Lu, F.; Yager, K. G.; Van Der Lelie, D.; Gang, O. A general strategy for the DNA-mediated self-assembly of functional nanoparticles into heterogeneous systems. *Nat. Nanotechnol.* **2013**, *8*, 865−872.

(53) Zhang, Y.; Pal, S.; Srinivasan, B.; Vo, T.; Kumar, S.; Gang, O. Selective transformations between nanoparticle superlattices via the reprogramming of DNA-mediated interactions. *Nat. Mater.* **2015**, *14*, 840−847.

(54) Vo, T.; Venkatasubramanian, V.; Kumar, S.; Srinivasan, B.; Pal, S.; Zhang, Y.; Gang, O. Stoichiometric control of DNA-grafted colloid self-assembly. *Proc. Natl. Acad. Sci. U. S. A.* **2015**, *112*, 4982−4987.

(55) Wang, S.; Lee, S.; Du, J. S.; Partridge, B. E.; Cheng, H. F.; Zhou, W.; Dravid, V. P.; Lee, B.; Glotzer, S. C.; Mirkin, C. A. The emergence of valency in colloidal crystals through electron equivalents. *Nat. Mater.* **2022**, *21*, 580−587.

(56) Lesnyak, V.; Wolf, A.; Dubavik, A.; Borchardt, L.; Voitekhovich, S. V.; Gaponik, N.; Kaskel, S.; Eychmüller, A. 3D assembly of semiconductor and metal nanocrystals: hybrid CdTe/Au structures with controlled content. *J. Am. Chem. Soc.* **2011**, *133*, 13413−13420.

(57) Sherman, Z. M.; Green, A. M.; Howard, M. P.; Anslyn, E. V.; Truskett, T. M.; Milliron, D. J. Colloidal nanocrystal gels from thermodynamic principles. *Acc. Chem. Res.* **2021**, *54*, 798−807.

(58) Green, A. M.; Ofosu, C. K.; Kang, J.; Anslyn, E. V.; Truskett, T. M.; Milliron, D. J. Assembling inorganic nanocrystal gels. *Nano Lett.* **2022**, *22*, 1457−1466.

(59) Sherman, Z. M.; Kim, K.; Kang, J.; Roman, B. J.; Crory, H. S. N.; Conrad, D. L.; Valenzuela, S. A.; Lin, E. Y.; Dominguez, M. N.; Gibbs, S. L.; et al. Plasmonic response of complex nanoparticle assemblies. *ChemRxiv* **2022**, DOI: 10.26434/chemrxiv-2022-rkqw8.

(60) Shih, W.-H.; Liu, J.; Shih, W.; Kim, S.; Sarikaya, M.; Aksay, I. Mechanical properties of colloidal gels. *Mater. Res. Soc. Symp. Proc.* **1989**, *155*, 83−92.

(61) Rueb, C. J.; Zukoski, C. F. Viscoelastic properties of colloidal gels. *J. Rheol.* **1997**, *41*, 197−218.

(62) Del Gado, E.; Fiocco, D.; Foffi, G.; Manley, S.; Trappe, V.; Zaccone, A. *Fluids, Colloids and Soft Materials: An Introduction to Soft Matter Physics*; John Wiley & Sons: Hoboken, NJ, 2016.

(63) Song, J.; Rizvi, M. H.; Lynch, B. B.; Ilavsky, J.; Mankus, D.; Tracy, J. B.; McKinley, G. H.; Holten-Andersen, N. Programmable anisotropy and percolation in supramolecular patchy particle gels. *ACS Nano* **2020**, *14*, 17018−17027.

(64) Howard, M. P.; Jadrich, R. B.; Lindquist, B. A.; Khabaz, F.; Bonnecaze, R. T.; Milliron, D. J.; Truskett, T. M. Structure and phase behavior of polymer-linked colloidal gels. *J. Chem. Phys.* **2019**, *151*, 124901.

(65) Howard, M. P.; Sherman, Z. M.; Sreenivasan, A. N.; Valenzuela, S. A.; Anslyn, E. V.; Milliron, D. J.; Truskett, T. M. Effects of linker flexibility on phase behavior and structure of linked colloidal gels. *J. Chem. Phys.* **2021**, *154*, 074901.

(66) Kondo, S.; Sakurai, H.; Chung, U.-i.; Sakai, T. Mechanical properties of polymer gels with bimodal distribution in strand length. *Macromolecules* **2013**, *46*, 7027−7033.

(67) Di Lorenzo, F.; Seiffert, S. Nanostructural heterogeneity in polymer networks and gels. *Polym. Chem.* **2015**, *6*, 5515−5528.

(68) Sakai, T.; Matsunaga, T.; Yamamoto, Y.; Ito, C.; Yoshida, R.; Suzuki, S.; Sasaki, N.; Shibayama, M.; Chung, U.-i. Design and fabrication of a high-strength hydrogel with ideally homogeneous network structure from tetrahedron-like macromonomers. *Macromolecules* **2008**, *41*, 5379−5384.

(69) Akagi, Y.; Gong, J. P.; Chung, U.-i.; Sakai, T. Transition between phantom and affine network model observed in polymer gels with controlled network structure. *Macromolecules* **2013**, *46*, 1035−1040.

(70) Plimpton, S. Fast parallel algorithms for short-range molecular dynamics. *J. Comput. Phys.* **1995**, *117*, 1−19.
(71) Rubinstein, M.; Colby, R. H. *Polymer Physics*; Oxford University Press: New York, 2003; Vol. *23*.
(72) Stukowski, A. Visualization and analysis of atomistic simulation data with OVITO−the Open Visualization Tool. *Model Simul. Mater. Sci. Eng.* **2010**, *18*, 015012.
(73) Lindbo, D.; Tornberg, A.-K. Fast and spectrally accurate Ewald summation for 2-periodic electrostatic systems. *J. Chem. Phys.* **2012**, *136*, 164111.
(74) Jadrich, R. B.; Bollinger, J. A.; Lindquist, B. A.; Truskett, T. M. Equilibrium cluster fluids: Pair interactions via inverse design. *Soft Matter* **2015**, *11*, 9342−9354.
(75) Lio, G. E.; Palermo, G.; Caputo, R.; De Luca, A. Opto-mechanical control of flexible plasmonic materials. *J. Appl. Phys.* **2019**, *125*, 082533.
(76) Sherman, Z. M.; Howard, M. P.; Lindquist, B. A.; Jadrich, R. B.; Truskett, T. M. Inverse methods for design of soft materials. *J. Chem. Phys.* **2020**, *152*, 140902.
(77) Schreiber, R.; Do, J.; Roller, E.-M.; Zhang, T.; Schüller, V. J.; Nickels, P. C.; Feldmann, J.; Liedl, T. Hierarchical assembly of metal nanoparticles, quantum dots and organic dyes using DNA origami scaffolds. *Nat. Nanotechnol.* **2014**, *9*, 74−78.
(78) Ferreiro-Córdova, C.; Del Gado, E.; Foffi, G.; Bouzid, M. Multi-component colloidal gels: interplay between structure and mechanical properties. *Soft Matter* **2020**, *16*, 4414−4421.
(79) Ye, X.; Chen, J.; Diroll, B. T.; Murray, C. B. Tunable plasmonic coupling in self-assembled binary nanocrystal superlattices studied by correlated optical microspectrophotometry and electron microscopy. *Nano Lett.* **2013**, *13*, 1291−1297.
(80) Cargnello, M.; Johnston-Peck, A. C.; Diroll, B. T.; Wong, E.; Datta, B.; Damodhar, D.; Doan-Nguyen, V. V. T.; Herzing, A. A.; Kagan, C. R.; Murray, C. B. Substitutional doping in nanocrystal superlattices. *Nature* **2015**, *524*, 450−453.
(81) Shi, Q.; Sikdar, D.; Fu, R.; Si, K. J.; Dong, D.; Liu, Y.; Premaratne, M.; Cheng, W. 2d binary plasmonic nanoassemblies with semiconductor n/p-doping-like properties. *Adv. Mater.* **2018**, *30*, 1801118.
(82) Jishkariani, D.; Elbert, K. C.; Wu, Y.; Lee, J. D.; Hermes, M.; Wang, D.; van Blaaderen, A.; Murray, C. B. Nanocrystal core size and shape substitutional doping and underlying crystalline order in nanocrystal superlattices. *ACS Nano* **2019**, *13*, 5712−5719.
(83) Ninarello, A.; Ruiz-Franco, J.; Zaccarelli, E. Onset of criticality in hyper-auxetic polymer networks. *Nat. Commun.* **2022**, *13*, 1−8.

## Recommended by ACS

**Buckling and Interfacial Deformation of Fluorescent Poly(*N*-isopropylacrylamide) Microgel Capsules**
Fabian Hagemans, Walter Richtering, *et al.*
APRIL 13, 2023
ACS NANO
READ

**Dynamic Heterogeneity in the Optical Signals from Single Nano-Objects**
Michel Orrit.
APRIL 28, 2023
THE JOURNAL OF PHYSICAL CHEMISTRY B
READ

**Free Energy Contributions to the Template-Assisted Self-Assembly of Nanoparticles Using Steered Molecular Dynamics Simulations: Implications for Molecular-Specifi...**
Zhen Luo and Shafigh Mehraeen
DECEMBER 19, 2022
ACS APPLIED NANO MATERIALS
READ

**Quantitative Acoustophoresis**
Vadim Bogatyr, Gijs J. L. Wuite, *et al.*
JUNE 22, 2022
ACS NANOSCIENCE AU
READ

**Get More Suggestions >**